ACS APPLIED MATERIALS & INTERFACES

Research Article

www.acsami.org

Periodic Parallel Array of Nanopillars and Nanoholes Resulting from Colloidal Stripes Patterned by Geometrically Confined Evaporative Self-Assembly for Unique Anisotropic Wetting

Xiangmeng Li, Chunhui Wang, Jinyou Shao,* Yucheng Ding,* Hongmiao Tian, Xiangming Li, and Li Wang

Micro- and Nanotechnology Research Center, State Key Laboratory for Manufacturing Systems Engineering, Xi'an Jiaotong University, Xi'an, Shaanxi 710049, China

Supporting Information

ABSTRACT: In this paper we present an economical process to create anisotropic microtextures based on periodic parallel stripes of monolayer silica nanoparticles (NPs) patterned by geometrically confined evaporative self-assembly (GCESA). In the GCESA process, a straight meniscus of a colloidal dispersion is initially formed in an opened enclosure, which is composed of two parallel plates bounded by a U-shaped spacer sidewall on three sides with an evaporating outlet on the fourth side. Lateral evaporation of the colloidal dispersion leads to periodic "stick–slip" receding of the meniscus (evaporative front), as triggered by the "coffee-ring" effect, promoting the assembly of silica NPs into periodic parallel stripes. The morphology of stripes can be well controlled by tailoring process variables such as substrate wettability, NP concentration, temperature, and gap height, etc. Furthermore, arrayed patterns of nanopillars or nanoholes are generated on a silicon wafer using the as-prepared colloidal stripes as an etching mask or template. Such arrayed patterns can reveal unique anisotropic wetting properties, which have a large contact angle hysteresis viewing from both the parallel and perpendicular directions in addition to a large wetting anisotropy.

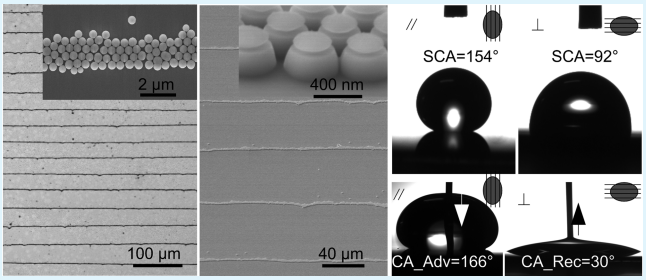

KEYWORDS: *silica nanoparticles, stripe patterns, geometrically confined evaporative self-assembly, nanopillar array, nanohole array, anisotropic wetting*

INTRODUCTION

Nanoparticle crystals represent a building block for nanotechnologies. Specifically, a regular stripe-shaped pattern of nanoparticles (NPs) can find potential applications in surface engineering,[1−3] optoelectronics,[4−7] biotechnology,[8] etc. Numerous methods have been exploited to pattern NPs into such functional structures, including e-jet printing,[9] micro contact printing,[10] nanopipetting,[11] template-directed assembly,[12,13] nanolithography,[14] optical trapping assembly,[15] and electrically and magnetically induced assembly,[16,17] which are mostly based on self-assembly of various NPs from a colloidal dispersion. Evaporative or convective self-assembly approaches[18−20] have attracted great attention from researchers as high-throughput and nonlithographic techniques for patterning spatially ordered stripes or hierarchical structures.

In a typical evaporative self-assembly process implemented with a colloidal dispersion, a convective force is induced by solvent evaporation and tends to transport NPs from the colloid toward the solid–liquid–vapor triple-phase contact line (TPCL), triggered by the "coffee-ring" effect.[21] The TPCL, as an evaporative front, receding progressively in a "stick–slip" mode, can lead to deposition of NPs into a cluster of stripes perpendicular to the receding direction. Various geometrical confinements can be employed to affect such a flow-coating process of NPs over a substrate for generating patterns of NPs with a well-controllable hierarchy or morphology. For example, Lin's group developed self-assembly processes using curve-to-flat or wedge-shaped confinements to obtain inorganic,[22,23] polymeric,[24,25] or biomaterial[26] patterns for potential applications in optoelectronics, solar-energy harvesting, and fluorescent biosensing. The geometric confinements proposed so far could mostly generate regularly distributed rings with a morphological gradient.

For some unique applications, such as anisotropically wetting surfaces,[27−29] for instance, periodic and parallel microtextures would be highly desirable for a spatially uniform wettability. Recently, many groups have developed a variety of approaches to obtain such highly regular and uniform patterns.[30−34] Dip-coating can achieve well-aligned stripe patterns with a dilute solution of polymer-coated NPs.[30] This technique cannot precisely control the stripe morphology due to the instability inherent to the solvent during the evaporation,[31] whereas

Received: August 28, 2014
Accepted: October 29, 2014
Published: October 29, 2014

another type of flow-coating approach with horizontal convective self-assembly can generate well-defined stripe and grid patterns of NPs by precise control of the position and translation of the meniscus.[32] This work was followed by a similar approach in which a vertical convective self-assembly was proposed and NP stripes of the desired periodicity and spacing could be obtained by manipulating the liquid level.[33] Although these methods can achieve highly ordered periodic NP stripes in a controlled manner, the control of the morphologies of the NP stripes is realized via certain apparatus-like programmable motors. In addition, a well-distributed colloidal stripe array can also be created by transfer from a monolayer or multilayer of colloidal films using soft lithography.[34] However, this approach requires preparation of a colloidal film in advance, as well as a prepatterned poly(dimethylsiloxane) (PDMS) template which is fabricated on the basis of conventional lithography.

In this paper, a simple strategy is presented for creating a periodic and parallel array of nanopillars and nanoholes, resulting from monolayer stripes of colloidal NPs, which are patterned by geometrically confined evaporative self-assembly (GCESA). Compared with the existing methods, the proposed GCESA method does not need any apparatus-like motors to control the motion of the plates, except for arrangement of the parallel plates with a varied spacer height and adjustment of some conditions such as colloidal concentration, temperature, etc. to realize fabrication of various periodicities and widths of NP stripes. Thus, the proposed GCESA method can be a cost-effective alternative approach for patterning stripelike microstructures with colloidal NPs. Different from the two-plate geometric confinement where the movement of the meniscus and control of the deposition of nonvolatile solutes are based on the translation of the upper plate,[35] the proposed GCESA method is based on an immobilized two-plate confinement, i.e., an opened enclosure, which is composed of two parallel rectangular plates bounded by a U-shaped spacer sidewall on the three sides, leaving a microfluidic space with a gap-shaped outlet only on the fourth. The colloidal dispersion can evaporate more rapidly when subjected to heating, and a straight evaporative front is initiated at the outlet of the enclosure. A progressive and regular stick−slip receding motion of the evaporative front and parallel ordered stripes of the colloidal NPs can be observed. Besides, the silica NPs are robust enough to be used as an etching mask to silicon. Due to the low mechanical strength of the as-prepared colloidal stripes and their tendency to be removed easily, dry etching transfer is implemented similarly to nanosphere lithography as reported by Yang et al.[34] to produce a nanopillar or nanohole array on a silicon wafer with the colloidal stripes as an etching mask or template. Eventually, unique anisotropic wetting properties can be investigated on the resultant nanopillar and nanohole array surfaces.

EXPERIMENTAL SECTION

Preparation of Colloidal Particles. The monodispersed silica colloidal NPs used in this study were prepared by Stober's method using tetraethoxyorthosilicate (TEOS; 99.9%, Aldrich), ethanol (99.9%, Aldrich), and NH_4OH (28% NH_3 in water, Aldrich) as starting materials.[36] Briefly, these materials were mixed rapidly and stirred thoroughly at an intermediate speed overnight. Then the produced solution was purified by several cycles of centrifugation, decantation, and redispersion in absolute ethanol to remove undesirable reagents and to prevent further reaction. The synthesized silica NPs were preapared in two major sizes, 450 nm (i.e., large NPs) and 120 nm (i.e., small NPs) on average by varying the concentrations of NH_4OH. Finally, the silica NPs were redispersed into varied concentrations ranging from 0.5 to 2 mg mL^{-1}. Herein, silica NPs in an ethanol dispersion, instead of polystyrene (PS) latex NPs in an aqueous solution,[24] were chosen as the colloidal dispersion to obtain a close-packed crystalline monlayer, because ethanol enables a small contact angle (CA) and rapid evaporation owing to the relatively low surface tension and low boiling point as compared with the aqueous solution.

Preparation of Substrates. Fluorine-doped tin oxide (FTO)-coated glass (FTO for short), a glass slide, and a silicon wafer were cut into a rectangular shape, cleaned in an ultrasonic bath using acetone, ethanol, and Milli-Q water (18 MΩ cm) succesively, blow-dried in nitrogen, and baked in a 150 °C oven. Polyimide (Kapton) films with various thicknesses were cleaned, dried in an oven, and prepared as U-shaped spacers.

Formation of Colloidal Stripe Patterns. Scheme 1a shows the experimental setup for the proposed GCESA process. The enclosure is made of two parallel and rectangular plates (i.e., the cover and substrate as shown in Figure S1a; see the Supporting Information) which are separated by a U-shaped spacer sidewall on three sides (see Figure S1b, Supporting Information), creating a microfluidic gap in the enclosure with an opening on the fourth side. Specifically, the silicon wafer, glass slide, and FTO were arranged into different cover/substrate pairs with FTO as the same cover plate. A drop of colloidal dispersion was supplied from the outlet and fully filled the microfluidic gap of the enclosure. Then such a simple setup of cover/substrate pair replete with colloidal dispersion was shifted onto a hot plate at a constant temperature and allowed to evaporate.

Scheme 1. Experimental Setup for Fabricating the Colloidal Stripes, Nanopillar Array, and Nanohole Array[a]

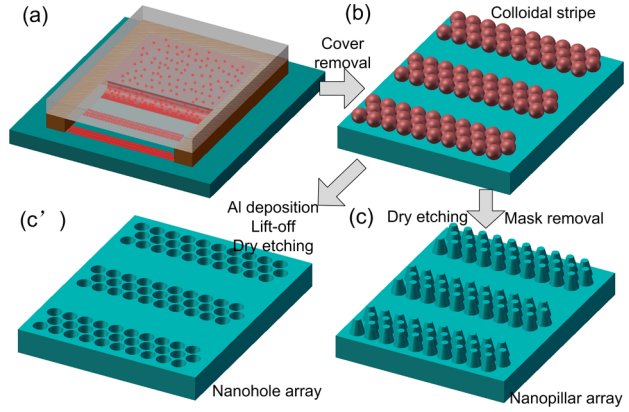

[a]Key: (a) proposed GCESA process, (b) colloidal stripes formation on the substrate, (c) nanopillar array formation on the silicon wafer by using the colloidal stripes as an etching mask, (c′) nanohole array formation on the silicon wafer by using the deposited aluminum layer as an etching mask after lift-off removal of the colloidal stripes.

Formation of Nanopillar and Nanohole Arrays. Parts c and c′ of Scheme 1 show the procedure of fabricating nanopillar and nanohole arrays with the obtained colloidal stripes as an etching mask or template. The nanopillar arrays were obtained by dry etching from the as-prepared colloidal stripes on a silicon wafer in the chamber of a PlasmaLab System100 (Oxford Instruments) with etchant gases of SF_6 and C_4F_8 at flow rates of 12 and 27 sccm, an RF power of 700 W, and a bias voltage of 25 V. The etching duration ranged from 30 to 120 s to produce nanopillar arrays with various morphologies. The nanohole arrays were formed by dry etching, similar to the fabrication procedure for nanopillar arrays, the main difference lying in the prior process of sputtering deposition of 100 nm thick aluminum and the lift-off process to remove the colloidal stripe template.

Sample Characterization. The morphologies of the colloidal stripe and nanopillar and nanohole array patterns were characterized by laser scanning confocal microscopy (Olympus, OLS4000) and field emission scanning electron microscopy (SU8010, Hitachi). The surface wettability of different substrates and the anisotropic wetting properties were characterized on the contact angle platform Data-physics (OCA20). The advancing and receding contact angles were obtained by capturing the maximum and minimum contact angles before the contact lines started to move, with 40 μL of water being squeezed out of or withdrawn from a 1000 μL microsyringe. The evaporation of a water droplet on the nanopillar array surface was implemented under ambient conditions at a temperature of 25 °C and humidity of 45% RH.

RESULTS AND DISCUSSION

Formation of Colloidal Stripes by the GCESA Process. Figure S2 (see the Supporting Information) demonstrates a representative stripe pattern of silica NPs on a silicon wafer, with an effective size of about 3 cm × 2 cm. The sample shows an array of periodic and straight stripes in the middle region (see Figure S2b), while the stripes in proximity to the sidewall are distorted locally due to an additional wetting of the receding evaporative front (see Figure S2c). The proposed GCESA process is applicable over a relatively large area (~cm^2), depending on the linear length of the straight evaporative front, which is equal to the width of the microfluidic gap.

The formation of NP stripes is mainly due to the stick−slip motion of the evaporative front of the colloidal dispersion confined in the microfluidic gap. Due to the confinement of the U-shaped sidewall, the evaporative front is initiated only along the straight edge of the opening. With a continuous evaporation of solvent, a replenishing flow occurs to compensate the solvent loss from the bulk dispersion, and the colloidal NPs are simultaneously transported toward the TPCL (see Figure S1c in the Supporting Information).[21] When the height of the meniscus on the substrate decreases with evaporation, the NPs traveling to the TPCL start to assemble into a stripe under capillary force, as was observed by Adachi et al.[37] Moreover, the already-deposited NPs pinning the substrate may hinder the receding motion of the evaporative front temporarily. As soon as the pinning force is overcome by surface tension, a slip motion of the evaporative front will take place, separated from the "broken neck" until a new pinning state is reached.[38] Meanwhile, the unpinned NPs are carried back to the bulk flow, leaving an NP stripe on the substrate. Due to the saturation of solvent vapor, equilibrium of the temperature and humidity distribution is established locally around the evaporative front,[39] producing a constant condition for continuous evaporation of solvent. Consequently, the evaporative front moving in a stick−slip mode recedes into the bulk dispersion vertically to the opening edge, resulting in a pattern composed of NP stripes. The stick−slip evolution of the evaporating front is clearly shown in movie S1 (Supporting Information).

The volume loss of solvent (ΔV) of the evaporative front is obviously dependent on the evaporation rate,[23,40] which is affected greatly by the temperature and gap height (H), while the receding speed of the evaporative front mainly affected by the surface wettability. Due to a uniform gap height and homogeneous surface wettability of the cover and substrate in the proposed GCESA process, a constant ΔV can be assumed for each stick−slip motion of the receding evaporative front by ignoring the slightly decreasing rate of solvent vapor convection over an increasing path from the receding evaporative front to the outlet. Therefore, a precisely periodic NP deposition into stripes becomes possible. Furthermore, each stripe of NPs will be straight along the evaporative front, except for its two very ends, at which the stripe can be locally distorted due to the additional surface interaction provided by the spacer sidewall. To this extent, a pattern of NPs in the form of periodic parallel stripes can be expected.

To investigate the controllability of the GCESA process, an experiment was conducted to examine the effect of the substrate wettability, NP mass concentration, temperature, and gap height, etc., on the stripe patterning with a silica colloidal dispersion.

Effect of the Substrate Wettability. The stick−slip motion of the colloidal dispersion on the substrate is essentially dependent on the initial contact angle (θ_i) and critical receding contact angle (θ_r) of the evaporative front (as denoted in the inset of Figure S1c, Supporting Information). Figure 1

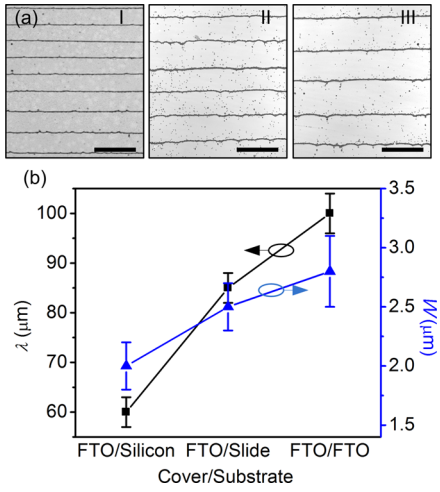

Figure 1. Effect of the substrate on the morphologies of the colloidal stripes. (a) Confocal microscopy images of the silica NP stripe pattern on silicon (I), glass slide (II), and FTO (III) substrates (at a gap height of 80 μm, a temperature of 65 °C, and an NP mass concentration of 1 mg mL^{-1}) (scale bar = 100 μm). (b) Dependence of the periodicity (λ) and width (W) of the colloidal stripes on the three substrates.

demonstrates comparative results obtained on different substrates. It can be seen that the periodicity and width of the stripe pattern formed on the FTO surface are larger than those of the stripe patterns obtained on both the slide and the silicon surfaces. This is mainly attributed to a difference in CA (receding hysteresis, defined as $\Delta\theta = \theta_i - \theta_r$) for different plate surfaces. With increasing CA difference, the periodicity and width of the colloidal stripes are increased nearly linearly. The result of the CA difference for a silica NP dispersion on different substrates is shown in Table S1 (Supporting Information). Due to the effect of the receding hysteresis, the slip motion occurs earlier for a silicon wafer compared to a glass slide or FTO. It is easier for the silica NPs to anchor the surface with a larger CA difference. The already-deposited silica NPs can also contribute to the adhesion and lead to a longer pinning time to increase the deposition width of the NP stripe. Specifically, the pinning time for each stripe formation is about 0.5 s for a silicon wafer, while it is about 1.0 s for a glass slide and 1.3 s for FTO. Therefore, a large loss of solvent will result in stripe patterns with a large periodicity. In this study, a silicon wafer is chosen as the substrate for fabrication of nanopillar and

nanohole array patterns for the sake of dry etching, as well as the tendency of forming stripes with a smaller width.

Effect of the NP Mass Concentration. Figure 2 shows the morphology of the patterned NP stripes related to the NP concentration. It is clearly seen that too low or too high a concentration can result in large periodicity stripes, while a smaller periodicity can be observed only in a range of properly selected concentration (Figure 2a). This is because, at a low concentration, the process needs more time to transport the silica NPs to the TPCL, and the probability of NP deposition is low; i.e., the initiation of NP deposition is delayed, corresponding to more loss of solvent and therefore to a large periodicity of the deposited stripes. At too high a concentration, on the other hand, it is easier for NPs to accumulate at the TPCL to assemble into a wider stripe (Figure 2b). At the same time, a larger number of silica NPs in the wide stripe generates a larger pinning force on the evaporative front so that it can stick for a longer time before its slip motion occurs driven by the surface tension. This corresponds to more volume loss and therefore to a larger periodicity of the stripes. In the following experiment, we should select a proper concentration, such as 1 mg mL^{-1}, to achieve a better morphology of the colloidal stripes.

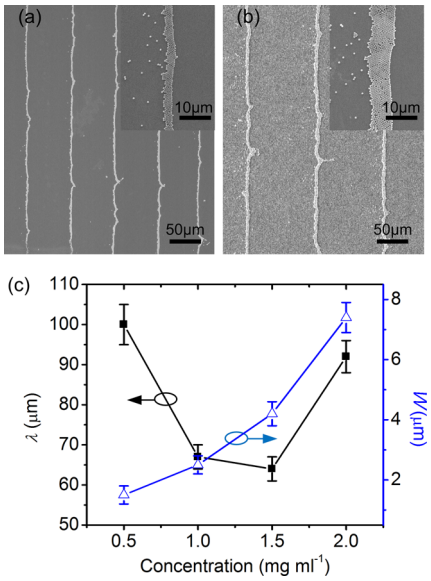

Figure 2. Effect of the concentration on the morphology of NP stripes formed on a glass slide. (a) and (b) show SEM images of the stripe pattern formed at concentrations of 1 and 2 mg mL^{-1}, respectively (with a gap height of 80 μm and a temperature of 65 °C). The inset images are the magnifications of the main images. (c) Dependence of the periodicity (λ) and width (W) of the colloidal stripes on the NP mass concentration.

Effect of the Temperature. The temperature is of great importance for the stripe formation using the GCESA strategy, because of its significant influence on the evaporation rate.[24] Figure S3 (Supporting Information) presents the confocal microscopy images of stripe patterns on a glass slide obtained at a temperature ranging from 30 to 70 °C. It is notable that only stochastic, discontinuous NP patterns are obtained at a relatively low temperature (see Figure S3a,b), while a pattern of increasingly regular stripes is formed with increasing temperature below the boiling point of the solvent (see Figure S3c,d). This is because a low temperature corresponds to a slow evaporation rate of the solvent, which tends to result in an irregular assembly of the silica NPs around the TPCL. Besides, the weakly pinning NPs are easily carried back to the bulk dispersion simultaneously with the slip motion due to the thermal circulation.[41] In contrast, as the temperature increases, a fast evaporation tends to drive a rapid accumulation of NPs to the TPCL owing to the fast replenishing flux. A subsequent fast hopping motion of the dispersion can therefore promote the deposition of a stripe pattern. It should also be noted that a recirculating flow can happen due to a temperature gradient from the cover to the warmer substrate, transporting the NPs toward the TPCL on the substrate.[41] The upper plate is cooler than the substrate surface, leading to a faster evaporative rate at the TPCL on the substrate than that of the upper plate, so that a driving force can occur on the colloidal dispersion to accumulate the NPs to the substrate. Meanwhile, it is observed that the solvent vapor can condense again on the cooler cover plate, resulting in a continuous residual liquid film which would move with the stick−slip receding motion and hinder the formation of colloidal stripes on the cover plate, as seen in Figure S1c (Supporting Information). Moreover, the colloidal dispersion used in this study is of low surface tension and low viscosity. Therefore, it is no doubt that stripes are not observed on the surface of the cover plate, different from the observation using high-viscosity solutions of polymers or macromolecules.[25,26]

Compared with the glass substrate, the range of feasible processing temperature for patterning straight stripes on a silicon wafer seems to be slightly larger due to the surface wettability, as shown in Figure 3. It can be also seen that the periodicity and vibration of the colloidal stripes formed at a temperature of 45 °C are larger than those the colloidal stripes formed at 65 °C for the same gap height, whereas the width of

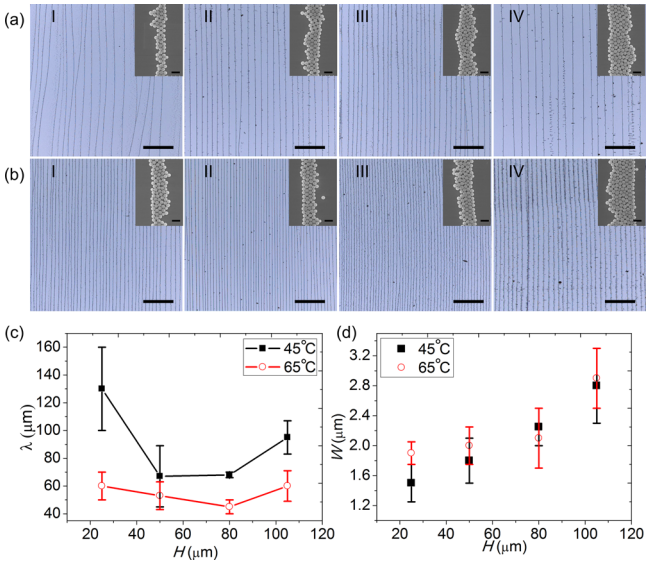

Figure 3. Effect of the temperature and gap height on the morphology of the colloidal stripes. (a, b) Confocal microscopy images of silica NP stripe patterns obtained on a silicon wafer at a varied gap height (H) of 25, 50, 80, and 105 μm, corresponding to I−IV, respectively, at temperatures of 45 °C (a) and 65 °C (b) and an NP mass concentration of 1 mg mL^{-1} (scale bar = 400 μm). The insets are the SEM images of the magnified stripes (scale bar = 2 μm). (c, d) Dependence of the stripe periodicity (λ) and width (W) on the gap height.

dx.doi.org/10.1021/am505835z | ACS Appl. Mater. Interfaces 2014, 6, 20300−20308

the stripes obtained at the two temperatures are similar to each other, as seen in Figure 3d.

Effect of the Gap Height. The gap height (H) between the plates is also a very important factor influencing the evaporative rate and the morphology of the stripe patterns. As shown in Figure 3, the stripe width increases monotonously with the gap height, a tendency different from that for the periodicity. The smallest periodicity (λ) can be found at a properly selected gap height (Figure 3c). There appears to be a nonlinear relationship between the periodicity and the gap height, indicating a nonlinear relationship between the gap height and the contact angle. On one hand, the larger periodicity obtained at a very small gap height may be due to the low probability of deposition with a lower amount of colloidal dispersion, which undergoes a complicated competition of the convective evaporation rate and the surface tension, which both depend nonlinearly on the gap height and determine the volume loss of solvent. On the other hand, the larger periodicity at a large gap height is due to the fact that a high evaporative rate can be produced with a large air−vapor interface area and a long pinning time due to more NPs probably deposited on the substrate, which both lead to a faster and a greater volume loss.

Variants of the GCESA Process. To investigate the versatility of the GCESA approach, multideposition of colloidal stripes was implemented. First, a gridlike pattern was achieved simply by performing a two-step GCESA. After the first round of deposition was accomplished and the substrate was cooled, the outlet of the enclosure was switched from one side of the rectangular plates to the orthogonal side, followed by a second deposition with the same process variables as those in the first round. Figure 4 shows the gridlike pattern formed by using the large silica NPs (Figure 4a). It can be clearly seen that the first patterned stripes are not affected by the second deposition, with the large NPs rearranged into a monolayer at the crossing point. Meanwhile, the latter deposited stripes are deformed slightly due to a frictional force on the former ones. During the second deposition using GCESA, the contact line can be wetted locally by the deposited stripes under a capillary force, thus leading to curved separated contact lines at the crossing point. Hence, the latter deposition of NP stripes is not strictly perpendicular to the former deposited stripes (see Figure S4 in the Supporting Information).

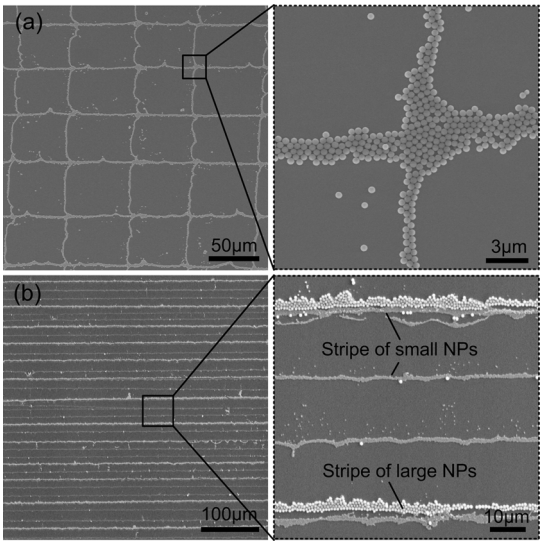

Figure 4. (a) Gridlike pattern obtained by two orthogonal depositions on a glass slide with large NPs (diameter of 450 nm, at an NP mass concentration of 1 mg mL^{-1}). (b) Hierarchical stripe pattern generated by two-step deposition with two different NPs (diameters of 450 and 120 nm, at a gap height of 80 μm, a temperature of 65 °C, and an NP mass concentration of 1 mg mL^{-1}). The right panels show the magnified SEM images for (a) and (b).

Moreover, a hierarchical structure was obtained by patterning of small and large NPs in a successive way (Figure 4b). It can be seen that the periodicity of the stripes patterned by large NPs is about 2 or 3 times that for the small NPs. Interestingly, the stripe patterns of large NPs are inclined to get close to one of the small NPs instead of settling between stripes of large NPs. This is due to the similar interactions of capillary force between the contact lines of latter deposition of large NPs and the previously formed stripes of small NPs during the stick−slip motion.

The low periodicity of small NP stripe deposition is due to diffusion dominating convection in the dispersion,[39] so that the small NPs travel and accumulate at the evaporative front at a faster speed than large NPs. Besides, the smaller pinning force exerted by the thinner layer of small NPs results in a decreased loss of solvent. Table S1 (Supporting Information) also implies that the CA difference $\Delta\theta$ is lower for the small NPs than that for the large NPs, leading to a smaller periodicity of colloidal stripes.

It is believed that the proposed GCESA is a versatile method and is also suitable for many other NPs such as polymer latex, metal colloids, core−shell NPs, and semiconductor quantum dots, etc. Figure 5 presents the patterned stripes of silica−gold core−shell NPs and silver NPs on a silicon wafer using the GCESA method. It was found that the formed stripe patterns of core−shell NPs and silver NPs are not a close-packed monolayer as the stripes of silica NPs. The difference in morphologies can be attributed to the effect of the complex combination of colloidal dispersions, e.g., the size, density, or dispersive properties.

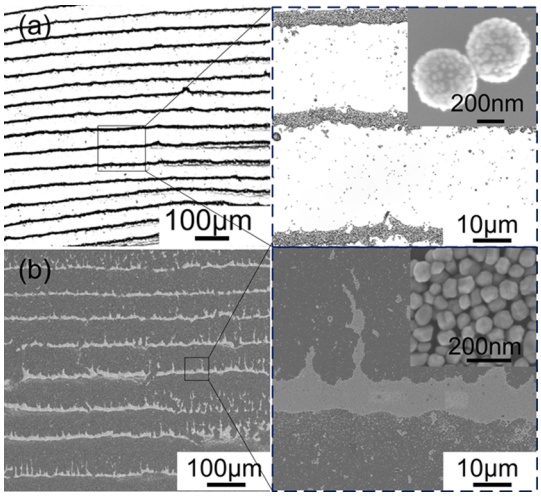

Figure 5. Deposition of functional colloidal NPs using the proposed GCESA method. (a) Microscopic image of SiO_2@Au core−shell NP stripes. (b) SEM images of silver NP stripes.

The proposed GCESA method is also believed to be an effective method for patterning stripelike microstructures with many functional colloidal NPs. The resulting NP patterns have

many potential applications, such as on antireflective films, superhydrophobic surfaces, light scattering films, and transparent conductive films, in surface plasmonic resonance detection, and so forth.[1−8] In our future work, it is necessary to investigate this GCESA approach to achieve ordered patterns of various functional NPs.

Besides, the reported NP patterns can be exploited for a kind of nanosphere lithography. In comparison, the photolithographic method can easily achieve highly ordered array patterns on surfaces over large areas.[28] For instance, in our previous work, microbowl array patterns fabricated on negative resist using electron beam lithography revealed highly adhesive hydrophobic wetting properties.[42] However, the proposed GCESA method can help achieve some unique micropatterns, e.g., hierarchical stripes and nanopillar or nanohole array patterns by further etching processes. The reported microstructures may also have some unique surface wetting properties due to their unique hierarchical morphologies.

Formation of Nanopillar and Nanohole Array Patterns and Their Anisotropic Wetting Properties. On the basis of the preceding results, it is easy to achieve periodic ordered stripe patterns of monolayer NPs with controllable periodicity and width by fine-tuning one of these process variables. Considering the ordered hierarchy of properties, the colloidal stripes on a silicon wafer can be utilized as an etching mask or template to form nanopillar and nanohole array patterns.

Figure 6 shows the nanopillar array patterns formed by varied etching durations. It is found that the morphology of the nanopillar array is determined by the etching duration. Generally, the height of the resultant nanopillars is increased with longer etching duration, while the top diameter is reduced simultaneously. The variation in morphology can lead to different anisotropic wetting behaviors, as shown in Table 1. In addition, a representative demonstration of anisotropic wetting properties on the nanopillar array surface is shown in Figure 6b,c. The anisotropy of wetting is about 62°, and more importantly, the contact angle hysteresis (CAH) is rather obvious in both the parallel and perpendicular directions, with values of about 136° and 68°, respectively.

Moreover, the nanohole array, as another hierarchical microtexure, was fabricated by a dry etching process similar to that for the nanopillar array fabrication after aluminum deposition and lift-off. As seen in Figure 7, the nanohole array patterns also reveal a wetting behavior similar to that of the nanopillar array surface, with wetting anisotropy of about 60° and CAHs of 120° and 52° for the parallel and perpendicular directions, respectively. It is clearly shown that for both the nanopillar array and nanohole array, the measured advancing CAs are near the static CAs, while the receding CAs are far below the static CAs viewing from both the parallel and perpendicular directions.

For both the nanopillar array and nanohole array, it is found that a water drop flows more easily over the microarrays with small periodicity. Taking the nanopillar array as an example, on one hand, a smaller static CA is found for smaller periodicity, especially viewing from the parallel direction, as seen in Figure 8. Meanwhile, it is also clearly shown that the static CA viewing from the perpendicular direction slightly increases with increasing periodicity. On the other hand, a large width tends to lead to a high energy barrier, which would be more robust to stop water from spreading laterally in the perpendicular direction, thus resulting in a larger static CA for a larger width, as seen in Figure 8c,d. By this means, the anisotropic

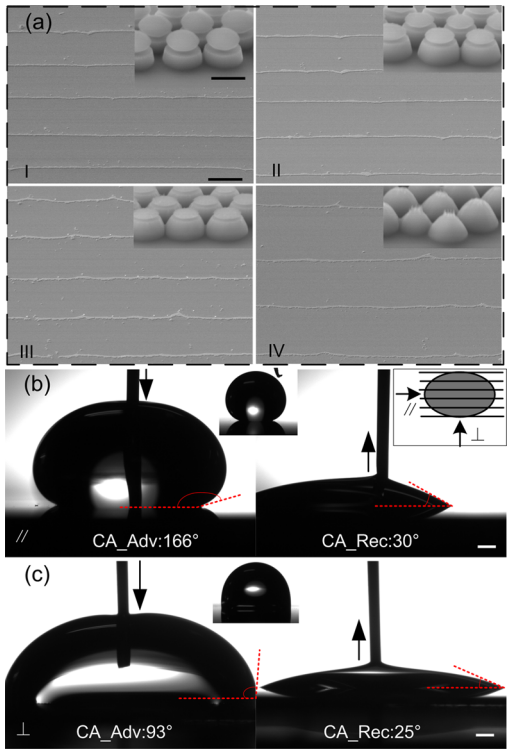

Figure 6. Nanopillar array patterns formed on a silicon wafer and representative anisotropic wetting properties. (a) Side-view SEM image of the nanopillar array obtained by dry etching with varied duration of 30, 60, 90, and 120 s for I–IV, respectively (with the residual silica unremoved) (scale bar = 40 μm). The insets are magnifications of the main images (scale bar = 400 nm). (b) Advancing and receding contact angle measurements viewing from the parallel direction. (c) Advancing and receding contact angle measurements viewing from the perpendicular direction. The insets in (b) and (c) show the shapes of the water drop in the static wetting state with values of 154° and 92°, respectively (scale bar = 1 mm).

Table 1. Anisotropic Wetting Properties Related to the Morphologies of the Nanopillar Array (NPA)[a]

NPA sample	etching duration (s)	height (nm)	D_{top} (nm)	$CA_{\parallel}$ (deg)	$CA_{\perp}$ (deg)	$CAH_{\parallel}$ (deg)	$CAH_{\perp}$ (deg)
1	30	225	400	154	92	136	68
2	60	330	285	140	92	115	61
3	90	375	175	128	91	97	51
4	120	390	50	116	89	70	39

[a] D_{top} is the top diameter of the nanopillars, $CA_{\parallel}$ and $CA_{\perp}$ are static contact angles viewing from the parallel and perpendicular directions, respectively, and $CAH_{\parallel}$ and $CAH_{\perp}$ are contact angle hystereses viewing from the parallel and perpendicular directions, respectively.

wetting properties can be modulated almost in a unidirectional manner by tailoring the morphologies of the nanopillar array patterns.[29]

The unique anisotropic wetting properties of these nanopillar or nanohole array patterns can be attributed to the energy barrier encountered in the parallel and perpendicular directions. Different from the grooved or striped patterns created by conventional lithography,[28] the reported patterns are a kind of hierarchical structure composed of discontinuous nanopillar or nanohole arrays. The static wetting properties of the proposed array patterns and the conventional grooved surface are similar.

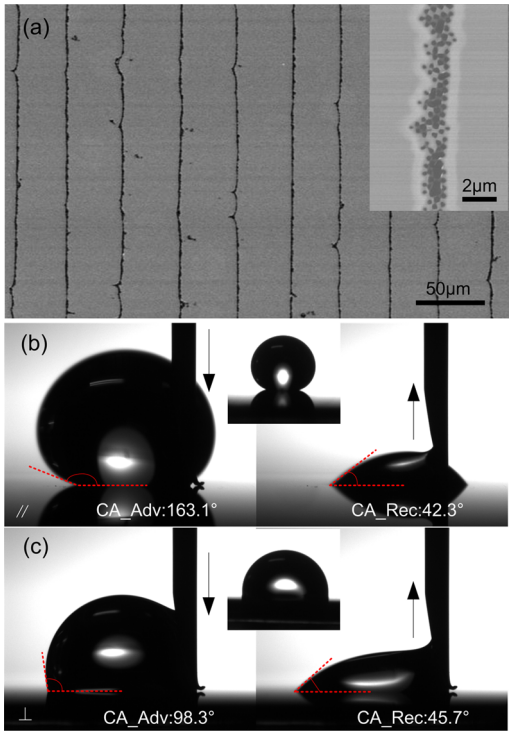

Figure 7. Nanohole array formed on a silicon wafer and the representative anisotropic wetting properties. (a) Top-view SEM image of the nanohole array pattern formed by aluminum deposition, lift-off removal of silica colloidal stripes, and dry etching. The insets are the magnifications of the SEM images. (b, c) The shapes of the water drops show the advancing and receding contact angles viewing from the parallel and perpendicular directions, respectively. The inset images are the static contact angles viewing from the parallel and perpendicular directions with values of 153° and 93°, respectively.

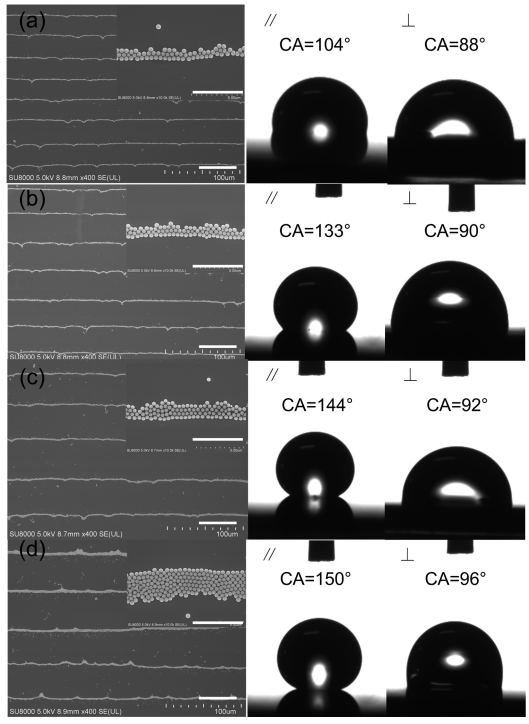

Figure 8. Static contact angle measurements on nanopillar array stripes with varied periodicity and width under the same etching duration of 60 s. The scale bars are 50 and 5 μm, respectively.

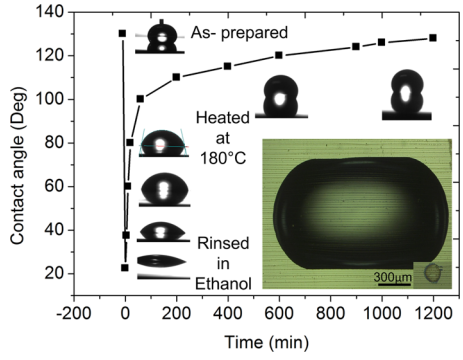

Figure 9. Effect of ethanol and thermal treatment on the switching wettability of the hierarchical nanopillar array pattern (generated from the colloidal stripe shown in Figure 4b) viewing from the parallel direction. The inset shows the shape of the evaporating water drop on the as-prepared surface and at the right corner, indicating the resultant pattern captured at the end of evaporation.

However, when it comes to the dynamic wetting properties, a much larger CAH is observed than that of the conventional grooved or striped patterns in both the parallel and perpendicular directions, due to the hierarchical morphologies of the microarrays. For the conventional grooved patterns, the energy barrier mainly exists in the perpendicular direction, while it is much less significant in the parallel direction. On the contrary, the proposed nanopillar and nanohole arrays indicate highly adhesive anisotropic wetting properties, mimicking the rice leaf and rose petal simultaneously. Such wetting properties are also different from those of the microbowl array pattern, acting only as a rose petal, with isotropic highly hydrophobic adhesive wetting properties.[42]

Finally, the switching wettability on the nanopillar array patterns was investigated. Figure 9 shows that the wettability of the hierarchical microarray formed by combined NP stripes (as seen in Figure 4b) can be alternated between high hydrophilicity by dipping in ethanol and hydrophobicity by thermal heating, with CA changing between 130° and 20°. Experiments were also performed on a flat silicon surface treated by the same etching process as well as on the nanopillar array resulting from only large NPs (as seen in Figure 8). For the latter pattern, the CA can change between 120° and 60° (see Figure S5a, Supporting Information), while, for the flat silicon surface, the CA range is from 92° to 65° and the recovery time is about 120 min (see Figure S5b, Supporting Information). Therefore, the switching wettability can be achieved on etched silicon surfaces with or without microtextures. Nonetheless, the hierarchical structure can provide abundant regular roughness favoring a larger range of switching CA, according to Wenzel's law.[43]

The possible mechanism for sucha phenomenon of switching wettability can be explained as follows. On one hand, the ethanol treatment forms an ultrathin layer of ethanol molecules on the surface of the silicon nanopillar array with enhanced affinity for water, so that the water drop can spread easily into the asperities of the nanopillar array, leading to a very small CA. On the other hand, the thermal treatment on a high-temperature hot plate (e.g., 180 °C) gradually evaporates the ethanol molecules and thus reduce the affinity for water. By this means, a large CA can be resumed due to the effect of the energy barrier of the nanopillar array. The switching wettability can therefore be observed by repeating the ethanol dipping and thermal treatment. By this means, insight into the switchable

wetting properties is provided. In addition, the evaporation evolution of the anisotropic wetting water droplet could eventually be reduced to a small pattern which is reminiscent of the most adhesive region during the evaporating process (see also movie S2, Supporting Information). From movie S2, it is found that, as soon as it reaches a state of critical receding with evaporation, the water drop starts to shrink along the parallel direction first and then along the perpendicular direction until it becomes round. Therefore, it can be inferred that there should be a very small amount of loss of water in the microfluidic transportation on such types of surfaces, due to the fact that the water droplet could retract easily from both the parallel and perpendicular directions.

Above all, the unique anisotropic wettability and switching of wetting states reported here on nanopillar and nanohole array surfaces is useful in applications of microfluidic transportation. In future work, it is necessary to further investigate these unique anisotropic wetting properties, which reveal a special biomimetic behavior of both rice leaf and rose petal at the same time.

CONCLUSION

In summary, we proposed an economical approach based on a GCESA for patterning nanoparticles into stripes which are spatially periodic and parallel in a dominant part of the effective patterning area and further transferred these colloidal stripes onto a silicon wafer simply by the dry etching process to achieve unique anisotropic wetting properties. The proposed GCESA process depends on an enclosure composed of two rectangular plates bounded by a U-shaped spacer sidewall, with an outlet only on one side of the rectangle. Such a geometric confinement produces a unidirectional convective evaporation of the colloidal dispersion of NPs, leading to an evaporative front receding in a periodic stick−slip mode laterally into the enclosure. Moreover, our experiment has demonstrated the controllability of the morphology of patterned stripes by tailoring several important process variables. The periodic parallel colloidal stripe patterns formed by the proposed GCESA method can be used as a mask to fabricate two different kinds of microtextures, namely, nanopillar and nanohole arrays, on the silicon wafer. Compared to the as-prepared colloidal stripes, the nanopillar and nanohole array patterns are mechanically robust, and importantly, they reveal unique anisotropic wetting properties with very high anisotropy in contact angle hysteresis as well as in the static contact angle, which are potentially useful in microfluidic transportation.

ASSOCIATED CONTENT

Supporting Information

Figures S1−S5 showing a schematic diagram of the GCESA process, confocal microscopy images of the obtained colloidal stripes, the temperature effect on patterning colloidal stripes, a schematic illustration of the effect of the former deposited stripes on the second deposited stripes, and switching wettability on a nanopillar array formed by large NPs only and a flat silicon wafer, Table S1 listing the contact angle difference on different substrates, and movies S1 and S2 illustrating the evolution of the colloidal stripe formation by GCESA and an evaporating water droplet on a hierarchical nanopillar array surface. This material is available free of charge via the Internet at http://pubs.acs.org.

AUTHOR INFORMATION

Corresponding Authors

*E-mail: jyshao@mail.xjtu.edu.cn.
*E-mail: ycding@mail.xjtu.edu.cn.

Notes

The authors declare no competing financial interest.

ACKNOWLEDGMENTS

This work was financed by the National Natural Science Foundation of China (NSFC) Major Research Plan on Nanomanufacturing (Grant 91323303), NSFC Funds (Grants 51175417 and 51275401), and Program for New Century Excellent Talents in University (Grant NCET-13-0454).

REFERENCES

(1) Luo, Y.; Wang, L.; Ding, Y. C.; Li, L.; Shi, J. F. High Light-Extracting Efficiency for OLED Directly Fabricated on Double-Side Nanotextured Silica Substrate. *Opt. Lett.* **2013**, *38*, 2394−2396.
(2) Ni, S. B.; Klein, M.; Spencer, N. D.; Wolf, H. Cascaded Assembly of Complex Multiparticle Patterns. *Langmuir* **2014**, *30*, 90−95.
(3) Wang, J. X.; Zhang, Y. Z.; Wang, S. T.; Song, Y. L.; Jiang, L. Bioinspired Colloidal Photonic Crystals with Controllable Wettability. *Acc. Chem. Res.* **2011**, *44*, 405−415.
(4) Layani, M.; Kamyshny, A.; Magdassi, S. Transparent Conductors Composed of Nanomaterials. *Nanoscale* **2014**, *6*, 5581−5591.
(5) Ding, T.; Song, K.; Clays, K.; Tung, C. H. Fabrication of 3D Photonic Crystals of Ellipsoids: Convective Self-Assembly in Magnetic Field. *Adv. Mater.* **2009**, *21*, 1936−1940.
(6) Su, B.; Zhang, C.; Chen, S.; Zhang, X.; Chen, L.; Wu, Y.; Nie, Y.; Kan, X.; Song, Y.; Jiang, L. A General Strategy for Assembling Nanoparticles in One Dimension. *Adv. Mater.* **2014**, *26*, 2501−2507.
(7) Sangeetha, N. M.; Decorde, N.; Viallet, B.; Viau, G.; Ressler, L. Nanoparticle-Based Strain Gauges Fabricated by Convective Self Assembly: Strain Sensitivity and Hysteresis with Respect to Nanoparticle Sizes. *J. Phys. Chem. C* **2013**, *117*, 1935−1940.
(8) Tran, V. T.; Zhou, H. J.; Kim, S.; Lee, J.; Kim, J.; Zou, F. M.; Kim, J.; Park, J. Y.; Lee, J. Self-Assembled Magnetoplasmonic Nanochain for DNA Sensing. *Sens. Actuators, B* **2014**, *203*, 817−823.
(9) Tse, L.; Barton, K. A Field Shaping Printhead for High-Resolution Electrohydrodynamic Jet Printing onto Non-Conductive and Uneven Surfaces. *Appl. Phys. Lett.* **2014**, *104*, 143510.
(10) Ombaba, M. M.; Logeeswaran, V. J.; Islam, M. S. Electrically Conducting Film of Silver Sub-Micron Particles as Mechanical and Electrical Interfaces for Transfer Printed Micro- and Nano-Pillar Devices. *Appl. Phys. A: Mater. Sci. Process.* **2013**, *111*, 251−259.
(11) Kim, J. T.; Spindler, S.; Sandoghdar, V. Scanning-Aperture Trapping and Manipulation of Single Charged Nanoparticles. *Nat. Commun.* **2014**, *5*, 3380.
(12) Meyerbroker, N.; Zharnikov, M. Hydrogel Nanomembranes as Templates for Patterned Deposition of Nanoparticles on Arbitrary Substrates. *ACS Appl. Mater. Interfaces* **2014**, *6*, 14729−14735.
(13) Zhai, S. J.; Jiang, Y. T.; Zhao, H.; Das, B. Direct Writing of Metallic Nanoparticle Concentric Multi-Ring Structures by Template-Directed Convective Self-Assembly Processes. *Adv. Opt. Mater.* **2014**, *2*, 632−635.
(14) Zhang, J. H.; Li, Y. F.; Zhang, X. M.; Yang, B. Colloidal Self-Assembly Meets Nanofabrication: From Two-Dimensional Colloidal Crystals to Nanostructure Arrays. *Adv. Mater.* **2010**, *22*, 4249−4269.
(15) Koniger, A.; Kohler, W. Optical Funneling and Trapping of Gold Colloids in Convergent Laser Beams. *ACS Nano* **2012**, *6*, 4400−4409.
(16) Mittal, M.; Furst, E. M. Electric Field-Directed Convective Assembly of Ellipsoidal Colloidal Particles To Create Optically and Mechanically Anisotropic Thin Films. *Adv. Funct. Mater.* **2009**, *19*, 3271−3278.
(17) Dai, Q.; Frommer, J.; Berman, D.; Virwani, K.; Davis, B.; Cheng, J. Y.; Nelson, A. High-Throughput Directed Self-Assembly of Core−

Shell Ferrimagnetic Nanoparticle Arrays. *Langmuir* **2013**, *29*, 7472−7477.
(18) Chen, K.; Stoianov, S. V.; Bangerter, J.; Robinson, H. D. Restricted Meniscus Convective Self-Assembly. *J. Colloid Interface Sci.* **2010**, *344*, 315−320.
(19) Arshad, T. A.; Bonnecaze, R. T. Templated Evaporative Lithography for High Throughput Fabrication of Nanopatterned Films. *Nanoscale* **2013**, *5*, 624−633.
(20) Han, W.; Lin, Z. Q. Learning from "Coffee Rings": Ordered Structures Enabled by Controlled Evaporative Self-Assembly. *Angew. Chem., Int. Ed.* **2012**, *51*, 1534−1546.
(21) Deegan, R. D.; Bakajin, O.; Dupont, T. F.; Huber, G.; Nagel, S. R.; Witten, T. A. Capillary Flow as the Cause of Ring Stains from Dried Liquid Drops. *Nature* **1997**, *389*, 827−829.
(22) Kwon, S. W.; Kim, T. Y.; Kim, Y.; Byun, M.; Lin, Z. Q.; Suh, K. S.; Yoon, D. H.; Yang, W. S. Micro-Patterns of Reduced Graphene Oxide (RG-O) Platelets Crafted by a Self-Assembled Template. *Soft Mater* **2011**, *7*, 6811−6815.
(23) Xu, J.; Xia, J. F.; Lin, Z. Q. Evaporation-Induced Self-Assembly of Nanoparticles from a Sphere-on-Flat Geometry. *Angew. Chem., Int. Ed.* **2007**, *46*, 1860−1863.
(24) Han, W.; Byun, M.; Lin, Z. Q. Assembling and Positioning Latex Nanoparticles via Controlled Evaporative Self-Assembly. *J. Mater. Chem.* **2011**, *21*, 16968−16972.
(25) Byun, M.; Bowden, N. B.; Lin, Z. Q. Hierarchically Organized Structures Engineered from Controlled Evaporative Self-Assembly. *Nano Lett.* **2010**, *10*, 3111−3117.
(26) Byun, M.; Han, W.; Li, B.; Hong, S. W.; Cho, J. W.; Zou, Q. Z.; Lin, Z. Q. Guided Organization of λ-DNA Into Microring Arrays From Liquid Capillary Bridges. *Small* **2011**, *7*, 1641−1646.
(27) Gleiche, M.; Chi, L. F.; Fuchs, H. Nanoscopic Channel Lattices with Controlled Anisotropic Wetting. *Nature* **2000**, *403*, 173−175.
(28) Xia, D. Y.; Brueck, S. Strongly Anisotropic Wetting on One-Dimensional Nanopatterned Surfaces. *Nano Lett.* **2008**, *8*, 2819−2824.
(29) Tanaka, D.; Buenger, D.; Hildebrandt, H.; Moeller, M.; Groll, J. Unidirectional Control of Anisotropic Wetting through Surface Modification of PDMS Microstructures. *Langmuir* **2013**, *29*, 12331−12336.
(30) Huang, J. X.; Kim, F.; Tao, A. R.; Connor, S.; Yang, P. D. Spontaneous Formation of Nanoparticle Stripe Patterns through Dewetting. *Nat. Mater.* **2005**, *4*, 896−900.
(31) Rabani, E.; Reichman, D. R.; Geissler, P. L.; Brus, L. E. Drying-Mediated Self-Assembly of Nanoparticles. *Nature* **2003**, *426*, 271−274.
(32) Kim, H. S.; Lee, C. H.; Sudeep, P. K.; Emrick, T.; Crosby, A. J. Nanoparticle Stripes, Grids, and Ribbons Produced by Flow Coating. *Adv. Mater.* **2010**, *22*, 4600−4604.
(33) Mino, Y.; Watanabe, S.; Miyahara, M. T. Colloidal Stripe Pattern with Controlled Periodicity by Convective Self-Assembly with Liquid-Level Manipulation. *ACS Appl. Mater. Interfaces* **2012**, *4*, 3184−3190.
(34) Zhang, X. M.; Zhang, J. H.; Ren, Z. Y.; Li, X.; Zhang, X.; Zhu, D. F.; Wang, T. Q.; Tian, T.; Yang, B. Morphology and Wettability Control of Silicon Cone Arrays Using Colloidal Lithography. *Langmuir* **2009**, *25*, 7375−7382.
(35) Yabu, H.; Shimomura, M. Preparation of Self-Organized Mesoscale Polymer Patterns on a Solid Substrate: Continuous Pattern Formation from a Receding Meniscus. *Adv. Funct. Mater.* **2005**, *15*, 575−581.
(36) Stober, W.; Fink, A.; Bohn, E. Controlled Growth of Monodisperse Silica Spheres in Micron Size Range. *J. Colloid Interface Sci.* **1968**, *26*, 62−69.
(37) Adachi, E.; Dimitrov, A. S.; Nagayama, K. Stripe Patterns Formed on a Glass-Surface during Droplet Evaporation. *Langmuir* **1995**, *11*, 1057−1060.
(38) Liu, N. L.; Zhou, Y.; Wang, L.; Peng, J. B.; Wang, J. A.; Pei, J. A.; Cao, Y. In Situ Growing and Patterning of Aligned Organic Nanowire Arrays via Dip Coating. *Langmuir* **2009**, *25*, 665−671.
(39) Leng, J. Drying of a Colloidal Suspension in Confined Geometry. *Phys. Rev. E* **2010**, *82*, 021405.
(40) Li, H.; Hain, T. C.; Muzha, A.; Schoppler, F.; Hertel, T. Dynamical Contact Line Pinning and Zipping During Carbon Nanotube Coffee Stain Formation. *ACS Nano* **2014**, *8*, 6417−6424.
(41) Ristenpart, W. D.; Kim, P. G.; Domingues, C.; Wan, J.; Stone, H. A. Influence of Substrate Conductivity on Circulation Reversal in Evaporating Drops. *Phys. Rev. Lett.* **2007**, *99*, 234502.
(42) Li, X. M.; Shao, J. Y.; Ding, Y. C.; Tian, H. M. Microbowl-Arrayed Surface Generated by EBL of Negative-Tone SU-8 for Highly Adhesive Hydrophobicity. *Appl. Surf. Sci.* **2014**, *307*, 365−371.
(43) Wenzel, R. N. Resistance of Solid Surfaces to Wetting by Water. *Ind. Eng. Chem.* **1936**, *28*, 988−994.